Topological edge states in the frequency dimension and their realization with Floquet electrical circuits

Alexander Stegmaier,[1,*] Alexander Fritzsche,[1] Riccardo Sorbello,[1] Martin Greiter,[1] Hauke Brand,[2] Christine Barko,[2] Maximilian Hofer,[2] Udo Schwingenschlögl,[3] Roderich Moessner,[4,5] Ching Hua Lee,[6,†] Alexander Szameit,[5,7] Andrea Alù,[8,9] Tobias Kießling,[2,5] and Ronny Thomale[1,5,‡]

[1]*Institute for Theoretical Physics and Astrophysics, University of Würzburg, Am Hubland, D-97074 Würzburg, Germany*
[2]*Physikalisches Institut and Röntgen Research Center for Complex Material Systems, Universität Würzburg, D-97074 Würzburg, Germany*
[3]*Physical Science and Engineering Division, King Abdullah University of Science and Technology (KAUST), Thuwal 23955, Saudi Arabia*
[4]*Max Planck Institute for the Physics of Complex Systems, Nöthnitzer Straße 38, 01187 Dresden, Germany*
[5]*Würzburg-Dresden Cluster of Excellence ct.qmat, D-97074 Würzburg, Germany*
[6]*Department of Physics, National University of Singapore, Singapore 117542, Singapore*
[7]*Institute of Physics, University of Rostock, Rostock, Germany*
[8]*Photonics Initiative, Advanced Science Research Center, City University of New York, New York, New York 10031, USA*
[9]*Physics Program, Graduate Center, City University of New York, New York, New York 10016, USA*

(Received 17 July 2024; revised 21 January 2025; accepted 23 September 2025; published 31 October 2025)

We build Floquet-driven capacitive circuit networks to realize topological states of matter in the frequency domain. As visible through our Floquet Laplacian formalism, the intertwining of static circuit components and parametric Floquet driving effectively creates a barrier in the frequency dimension, allowing to resolve the bulk-boundary correspondence of Floquet topological matter. By implementing a Su-Schrieffer-Heeger Floquet lattice model and measuring the associated circuit Laplacian and characteristic resonances, we demonstrate Floquet topological edge modes emerging at this frequency space barrier. Floquet circuits allow for the creation of topological phenomena in synthetic frequency dimensions with just a single unit cell of time-variable circuit components.

DOI: 10.1103/6n5m-wvs7

I. INTRODUCTION

Topological states of matter were initially explored within the realm of crystalline quantum materials. There, the bulk-boundary correspondence provides a deep connection between bulk topology, which is typically resolved in momentum space, and protected modes at edges or defects [1–5]. While the natural association with such a boundary would be some termination in real space, boundaries can likewise be realized in other spaces [6–10], which can be associated with modes featuring subextensive support in contrast to extensive bulk modes.

The manifestation of topological matter in abstract spaces and artificial dimensions has proliferated into metamaterial platforms [11]. In systems such as photonic waveguides, cavities, and ring resonators, artificial dimensions and topological signatures thereof embody the tunability of optical degrees of freedom [12–17] through utilizing mode dimensions [18–23], parameter modulations [9,24], or treating parameter space as an additional dimension [25]. Synthetic dimensions were also used in magneto-mechanical setups where topological pumping was observed [26] as well as atomic systems to study Bloch oscillations [27].

A fundamental resource providing nonspatial degrees of freedom is the time dimension, where periodic driving is readily used to create lattices in frequency space. Compared to real-space topological matter, frequency space realizations overcome certain limitations, e.g., naturally permitting nonlocal couplings through temporal engineering, and allow for higher-dimensional systems via multiple incommensurate driving frequencies [28–30]. Electronic circuits, ubiquitous in various technological domains, allow for a versatile design of effective frequency-dependent potentials and hopping terms. This is contrasted by the nature of Floquet platforms emulating the time-periodic Schrödinger equation, which are significantly more constrained.

In this article, we introduce the Floquet Laplacian formalism for parametrically driven circuits [31–34] and propose it as a framework to demonstrate lattice phenomena and topological features in the frequency dimension. We apply our approach to realize the topological edge states of the Su-Schrieffer-Heeger model within the frequency space. In order to observe topological edge states, we introduce an effective frequency boundary in our synthetic lattice; this

*Contact author: alexander.stegmaier@uni-wuerzburg.de
†Contact author: phylch@nus.edu.sg
‡Contact author: ronny.thomale@uni-wuerzburg.de

Published by the American Physical Society under the terms of the Creative Commons Attribution 4.0 International license. Further distribution of this work must maintain attribution to the author(s) and the published article's title, journal citation, and DOI.

has previously been a crucial challenge for the characterization of topological matter in frequency space, and has only been successfully addressed in optical ring resonators [6,7]. The frequency boundary is implemented in a system-inherent manner, i.e., using only those degrees of freedom that also constitute the topological state. We show how the dynamical properties of Floquet electrical circuits can be tailored through their topological signature, opening new avenues of topological circuit functionality.

II. FLOQUET LAPLACIAN FORMALISM

Electric circuits are a versatile metamaterial platforms to realize topological phenomena [35–44]. Typically, such experiments have relied on static circuit setups. By employing active elements [45] such as analog multipliers [32], however, we propose a convenient way to induce parametric driving while preserving full experimental tunability.

To derive the underlying theoretical framework, we consider a linear circuit network with a set of nodal voltages $V^i(t)$ and input currents $I^i(t)$. For a parametrically driven circuit element connecting the nodes i and j, let the current $I^{ij}(t)$ entering the element from node i be given by the integrodifferential equation

$$I^{ij}(t) = D_t^{\alpha} A^{ij}(t) D_t^{\beta} V^{ij}(t), \quad \alpha, \beta \in \mathbb{Z}. \tag{1}$$

Here, $V^{ij} = V^i - V^j$ is the voltage difference across the element and D_t^{ν} is the νth derivative for $\nu \geqslant 0$ or the $|\nu|$th antiderivative for $\nu < 0$ with respect to time. In an *L*-*R*-*C* circuit, ν takes the values -1, 0, and 1, respectively. $A^{ij}(t)$ is the coupling parameter associated with the circuit element. For a Floquet system with driving frequency Ω, it is time periodic so that $A^{ij}(t) = \sum_k A_k^{ij} \mathrm{e}^{\mathrm{i}k\Omega t}$. In the frequency domain, we can express Eq. (1) as

$$I_n^{ij}(\omega_0) = \sum_m (\mathrm{i}\omega_n)^{\alpha} (\mathrm{i}\omega_m)^{\beta} A_{n-m}^{ij} V_m^{ij}(\omega_0), \tag{2}$$

where $I_n^{ij}(\omega_0)$, $V_m^{ij}(\omega_0)$ are the Fourier components of $I^{ij}(t)$ and $V^{ij}(t)$ at the frequencies $\omega_n = \omega_0 + n\Omega$ and $\omega_m = \omega_0 + m\Omega$, respectively. Adding the currents flowing out of node i into connected circuit elements, we obtain $I_n^i(\omega_0) = \sum_j I_n^{ij}(\omega_0)$, the Fourier component at frequency ω_n of the input current. Then, we can arrange all contributions to the input current into an equation of the form

$$I_n^i(\omega_0) = \sum_{jm} \mathcal{J}_{nm}^{ij}(\omega_0) V_m^j(\omega_0), \tag{3}$$

where $\mathcal{J}_{nm}^{ij}(\omega_0)$ are the matrix elements of the Floquet Laplacian, a generalization of the circuit Laplacian [35]. We have delegated its full derivation to the Supplemental Material [46]. It is convenient to summarize the node indices i, j in vector form $\vec{I}_n(\omega_0) = \mathcal{J}_{nm}(\omega_0)\vec{V}_m(\omega_0)$. We see that the degrees of freedom coupled by the Floquet Laplacian are given by the frequencies $\{\omega_n = \omega_0 + n\Omega \mid n \in \mathbb{Z}\}$, which form a Bravais lattice, and the circuit nodes that constitute the sublattice [Fig. 1(a)]. ω_0 is formally equivalent to the quasienergy ϵ of the Floquet Schrödinger equation. It can be thought of as an offset of the Floquet lattice, but also takes on the role of the quasieigenfrequency of eigenmodes, which are the solutions to Eq. (3) with $\vec{I}_n(\omega_0) = 0$.

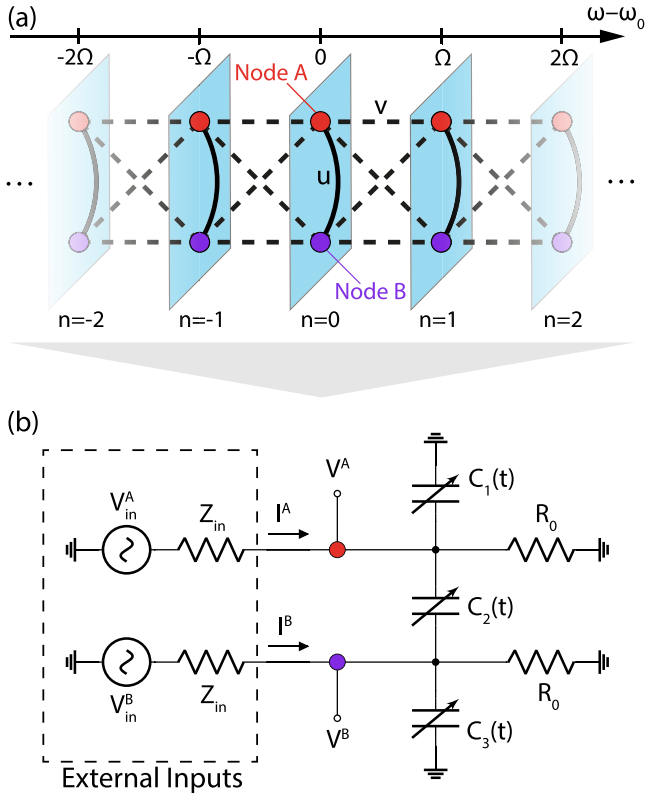


FIG. 1. (a) Floquet SSH model in frequency space. The SSH lattice is mapped onto intrasite coupling u (solid lines) connecting nodes A and B, and intersite couplings v (dashed lines) between neighboring frequency sites located at $n\Omega$. (b) Floquet SSH circuit. For each frequency, the two nodal voltages are V^{A} and V^{B}; the input currents of the circuit are I^{A} and I^{B}. Three capacitors $C_1(t)$, $C_2(t)$, and $C_3(t)$ constitute the time-varied capacitance matrix $\Gamma(t)$ in Eq. (4).

In principle, any circuit element such as resistors, inductors, or capacitors can be driven parametrically. This allows for diverse frequency dependencies in the Floquet Laplacian. In Eq. (2), arbitrary integer powers of $\mathrm{i}\omega$ occur, while our framework can be extended to also include rational functions and complex exponentials by introducing serial connections and time delay [46]. The frequency dependencies can appear both as an on-site potential and as coupling terms across circuit nodes and frequency components. This stands in contrast to the Floquet Schrödinger equation [47] $\sum_m (H_{n-m} + (\epsilon + n\Omega)\delta_{nm})|\psi_m(\epsilon)\rangle = 0$ that is limited to induce a periodic hopping model with a linear potential in the frequency domain.

III. FLOQUET SSH CIRCUIT WITH FREQUENCY BOUNDARY

We apply our framework to realize the topological edge states of the Su-Schrieffer-Heeger (SSH) model [2,48–50] in frequency space using a driven *C*-*R* circuit. The structure of the emergent circuit Floquet SSH lattice is shown in Fig. 1(a). At each frequency lattice site ω_n, there are two sublattice

sites A and B, which exhibit an equal-frequency coupling u. Furthermore, there are couplings between neighboring frequency sites denoted by v.

Our circuit realization of such a Floquet SSH model is sketched in Fig. 1(b). It has two circuit nodes that correspond to the sublattice sites in Fig. 1(a), carrying nodal voltages $\vec{V}(t) = (V^{\mathrm{A}}(t), V^{\mathrm{B}}(t))^{\intercal}$. At its core are three time-dependent capacitors, which are implemented based on four analog multipliers, so that the capacitances can be varied arbitrarily at high frequency through external control signals [46]. The two function generators with added serial impedances Z_{in} provide input currents $\vec{I}(t) = (I^{\mathrm{A}}(t), I^{\mathrm{B}}(t))^{\intercal}$, and the resistors R_0 to ground realize resistive on-site terms.

The capacitance matrix of our circuit $\Gamma(t)$ takes the form

$$\Gamma(t) = C_0\left[\begin{pmatrix} v\sin\Omega t & u + v\cos\Omega t \\ u + v\cos\Omega t & -v\sin\Omega t \end{pmatrix} + \gamma\mathbb{1}\right], \quad (4)$$

where γ describes an offset that is the time-averaged capacitance between each node and ground. The total current contributed by this is $\vec{I} = D_t\,\Gamma(t)\vec{V}(t)$. Choosing $\gamma > |u + v|$ ensures the dynamical stability of the circuit [46]. Up to a Pauli rotation, Eq. (4) corresponds to the conventional Bloch Hamiltonian representation of the SSH model. By analogy, the crystal momentum k is replaced by time t, and the driving frequency Ω plays the role of the lattice constant. The coupling parameters $u, v \in \mathbb{R}$ can be tuned via the control signals at the analog multipliers [46]. The resistors contribute a current $\vec{I}(t) = \Sigma\vec{V}(t)$ with $\Sigma = R_0^{-1}\mathbb{1}$.

After Fourier transformation, the C-R circuit differential equation reads

$$\frac{\vec{I}_n(\omega_0)}{\mathrm{i}(\omega_0 + n\Omega)} = \sum_m \left[\Gamma_{n-m} + \frac{1}{\mathrm{i}(\omega_0 + n\Omega)R_0}\delta_{nm}\mathbb{1}\right]\vec{V}_m(\omega_0) = \sum_m \tilde{\mathcal{J}}_{nm}\vec{V}_m(\omega_0), \quad (5)$$

where $\vec{I}_j(\omega_0)$ ($\vec{V}_j(\omega_0)$) is the jth component of the current (voltage) vector in the frequency lattice and $\tilde{\mathcal{J}}_{nm}$ is the normalized Floquet Laplacian ($\tilde{\mathcal{J}}_{nm} := \mathcal{J}_{nm}/(\mathrm{i}(\omega_0 + n\Omega))$). Its first term Γ_{n-m} corresponds to the $(n-m)$th Fourier component of Eq. (4) and forms a periodic hopping matrix coupling neighboring frequency lattice sites [Fig. 1(a)].

Importantly, for $\Omega \gg 1/(R_0C_0)$, the second term $\delta_{nm}/(\mathrm{i}(\omega_0 + n\Omega)R_0)$ on the right-hand side of Eq. (5) constitutes a potential barrier at $n = 0$ for $\omega_0 \approx 0$. This potential barrier emerges naturally from the differential equation and effectively decouples the zeroth node from its neighbors, thereby introducing boundaries at $n = \pm 1$. This is crucial for the observation of boundary phenomena, since the underlying model without the resistive term is fully translationally invariant in frequency space.

IV. OBSERVATION OF FREQUENCY SPACE TOPOLOGICAL SPECTRA

We experimentally obtain the normalized admittance spectrum of the Floquet SSH circuit, which are the eigenvalues of $\tilde{\mathcal{J}}(\omega_0)$. This is done by measuring the voltage response to different input currents across the Floquet lattice. As the frequency lattice is infinite, we introduce a frequency cutoff for experimental measurements. For this, we use a sampling rate that is an integer multiple of the driving frequency, so that through aliasing the frequency domain of the measured signals becomes compactified. We choose the sampling frequency such that we obtain a frequency lattice of 21 sites. Further, in the circuit setup, an offset $\gamma = 2$ [Eq. (4)] results in a shift along the real axis of $\tilde{j}$.

We distinguish the topologically trivial ($|u| > |v|$) from the nontrivial ($|u| < |v|$) case depicted in Figs. 2(a) and 2(b), respectively. Most of the normalized admittance eigenvalues $\tilde{j}$ lie in the vicinity of the real axis, where they form a two-band gapped spectral structure (marked black). The purple markers indicate two bound states of the barrier potential, which are separated from the remaining spectrum by an imaginary gap due to the high, imaginary-valued potential of the resistive term in Eq. (5). In the topological case [Fig. 2(b)], we observe

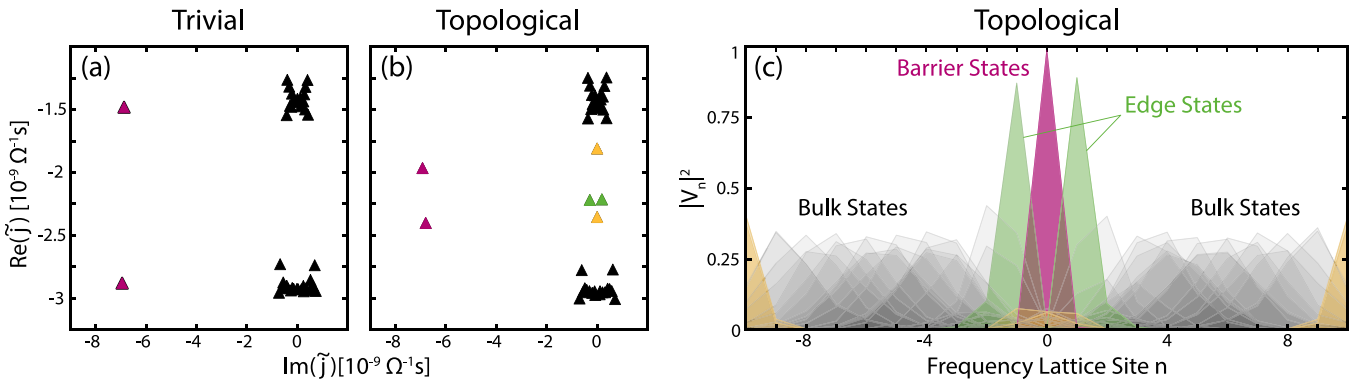


FIG. 2. Spectrum and eigenstates of the measured normalized Floquet Laplacian $\tilde{\mathcal{J}}(\omega_0)_{nm}$ of the circuit for $\omega_0 = 0.05\Omega$. (a) Spectrum of $\tilde{\mathcal{J}}(\omega_0)_{nm}$ for the topologically trivial case with $u = -0.75$ and $v = -0.25$. The barrier-bound states (purple) are clearly separated from the gapped bulk states (black). (b) Spectrum of $\tilde{\mathcal{J}}(\omega_0)_{nm}$ for the topologically nontrivial case with $u = -0.25$ and $v = -0.75$. Additional midgap states (green, yellow) are observed. (c) Weight distribution of the eigenstates of $\tilde{\mathcal{J}}(\omega_0)_{nm}$ in the frequency lattice for the topological case. The midgap states marked green are found to be exponentially localized adjacent to the potential barrier at $n = 0$, where the pair of bound barrier states (purple) resides. The midgap states marked yellow reside at the experimental frequency cutoff at $n = \pm 10$, so their presence is an artifact of our measurement protocol. The remaining states (black) spread over the bulk of the frequency lattice.

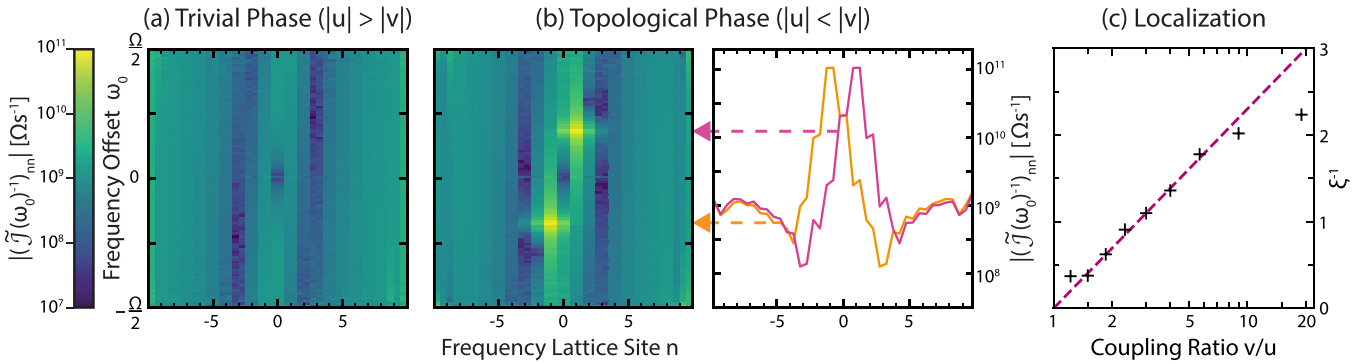


FIG. 3. Measured frequency sweep over the Floquet Brillouin zone of the on-site impedances over the Floquet lattice. At each frequency lattice site, the values for the sublattice circuit nodes A and B are shown. The absolute values of the diagonal entries of the inverse normalized Floquet Laplacian $|(\tilde{\mathcal{J}}(\omega_0))^{-1}_{nn}|$ scaled logarithmically for the topologically trivial (a) and topological (b) phases with $u = -0.75$, $v = -0.25$ and $u = -0.25$, $v = -0.75$, respectively. In the topological case, we observe resonance peaks that are exponentially localized at $n = \pm 1$. The right panel of plot (b) shows a horizontal cross section at the two ω_0 of maximum impedance, indicated by the dashed arrows. In the logarithmic representation, we observe an exponential decay with the distance from the frequency barrier. (c) Fitted inverse localization length ξ^{-1} for a set of measurements with different coupling ratios v/u. The observed resonance profiles (black markers) generally agree with the theoretical localization length of the SSH topological edge states (dashed line).

midgap states in between the bulk bands. By investigating the associated eigenvectors in Fig. 2(c), we find that the states marked yellow are localized at the artificial cutoff, and therefore not physical. The states marked green, however, localize at sites $n = \pm 1$ adjacent to the potential barrier, which effectively forms a boundary for the left and right regions of the lattice. They are topological frequency midgap edge states of the SSH model.

V. TOPOLOGICAL RESONANCES

In a second, independent measurement, we observe the signatures of the topological boundary states in frequency space by determining the resonances of the Floquet spectrum. Such resonances occur when the absolute value of an admittance eigenvalue of the Laplacian $|\tilde{j}_k|$ approaches 0. In the Floquet SSH model [Eq. (4)] with no offset, $\gamma = 0$, only the topological midgap states occur at approximately zero admittance. In the case of an ideal potential barrier at zero frequency, the resonances would correspondingly lie at $\omega_0 = 0$. Outside of this limit, they move to higher $|\omega_0|$ for decreasing R_0 as the potential broadens. In the circuit implementation, setting $\gamma = 0$ requires the introduction of an additional positive feedback that cancels constant on-site terms in the capacitance matrix [46]. We also use capacitors $C_{\text{in}} > C_0$ for the input impedances Z_{in} [see Fig. 1(b)] between the external voltage sources and the circuit nodes. This compensates the tendency of the circuit to become dynamically unstable for $\gamma < |u + v|$.

To determine the resonances of the Floquet circuit, we measure the Floquet Laplacian over the whole range of the Floquet Brillouin zone $\omega_0 \in [-\Omega/2, \Omega/2[$. Experimentally, this is done by using a set of harmonically modulated Gaussian pulses as input signals, in order to probe the entire Floquet Brillouin zone simultaneously. From the resulting measurements, we detect resonant modes by considering the diagonal elements of the inverse Floquet Laplacian, which are the impedances to ground at the different frequencies of the Floquet lattice:

$$(\tilde{\mathcal{J}}(\omega_0))^{-1}_{nn} = \langle n| \left(\sum_k \tilde{j}_k^{-1} |\psi_k\rangle\langle\psi_k| \right) |n\rangle = \sum_k \tilde{j}_k^{-1} |\langle n|\psi_k\rangle|^2 \approx \tilde{j}_{\text{res}}^{-1} |\langle n|\psi_{\text{res}}\rangle|^2, \quad (6)$$

where $|\psi_k\rangle$ are the eigenvectors of the Floquet Laplacian. The last approximation in Eq. (6) holds only if there is a resonant eigenvalue $|\tilde{j}_{\text{res}}| \approx 0$. We see that, in this case, the diagonal elements of the inverse Floquet Laplacian are approximately proportional to the profile of the resonant eigenmode in the frequency lattice.

The measured data are shown in Fig. 3. Since the admittance spectrum is never close to zero for the topologically trivial case [Fig. 3(a)], no resonances are observed. In the topological case [Fig. 3(b)], however, we find resonance peaks localized at the sites $n = \pm 1$, left and right of the barrier, in agreement with our prediction. Remarkably, the scale of the dominant resonance frequency is determined by the driving frequency Ω, and not by the characteristic frequency scale suggested by dimensional analysis, $\omega_{\text{ch}} = (R_0 C_0)^{-1}$. Hence, this principle allows for the control of the resonance frequency via the external driving signal: In the limit $\Omega \gg \omega_{\text{ch}}$ and full dimerization $u = 0$, $v = 1$, the resonant mode will be a harmonic oscillation at frequency Ω.

VI. FREQUENCY LOCALIZATION LENGTH

The topological edge states of the SSH model decay exponentially with the distance from the boundary, where the localization length ξ depends on the coupling ratio v/u. In the limit of $v/u \to \infty$, the topological modes are perfectly localized with $\xi = 0$. For decreasing v/u, the value of ξ increases and the states become fully delocalized as the band gap closes for $v/u \to 1$. To compare the localization length of the resonance profile to that of the SSH edge states, we repeat

the described resonance measurement procedure for different coupling ratios.

We determine ξ [compare Fig. 3(b), right panel] through a linear fit of the logarithm of the on-site impedances at the first three sites next to the barrier. Beyond $n = 3$, the impedance peaks drop off so much that they are overshadowed by contributions of other nonresonant states. The experimental results shown in Fig. 3(c) agree well with the theoretical prediction (denoted by the dashed purple line) for all but the lowest ($v/u = 11/9$) and the two highest ($v/u = 9$ and 19) investigated coupling ratios. The localization lengths for high coupling ratios deviate from the theory as contributions of nonresonant states become already significant for $|n| > 1$ as $\xi \ll 1$. In the case of coupling ratios close to 1, the band gap narrows, so that bulk modes at the band edges with eigenvalues $\tilde{j}$ approaching 0 influence the impedance profile. These results confirm that the profile of the measured resonant mode over the Floquet lattice exhibits the characteristic shape of the SSH topological edge state.

VII. CONCLUSIONS

We demonstrate how frequency space boundaries can naturally occur in periodically driven electric circuit networks as a result of the inhomogeneities intrinsic to the underlying Floquet Laplacian formalism. We used this unique property of Floquet circuits to experimentally realize and observe the topological boundary states of an SSH chain in frequency space. The unprecedented versatility of the underlying theoretical framework for Floquet circuits will enable the realization and study of a plethora of elusive frequency space topological phenomena, which are unattainable in most other experimental platforms due to the lack of accessible implementations of artificial boundaries. Moreover, the Floquet engineering enabled by periodically driven circuits yields compact devices as they are comprised of a single unit cell in real space. Their distinct dynamical properties can prove useful for applications, e.g., in analog signal processing, signal transmission, and sensing applications.

ACKNOWLEDGMENTS

The work was funded by the Deutsche Forschungsgemeinschaft (DFG, German Research Foundation) through Project No. 258499086—SFB 1170, the Würzburg-Dresden Cluster of Excellence on Complexity and Topology in Quantum Matter—*ct.qmat* Project No. 390858490—EXC 2147, the Ministry of Education, Singapore (MOE Award No. MOE-T2EP50222-0003), and through King Abdullah University of Science and Technology (KAUST).

[1] R. Jackiw and C. Rebbi, Solitons with fermion number ½, Phys. Rev. D **13**, 3398 (1976).
[2] W. P. Su, J. R. Schrieffer, and A. J. Heeger, Solitons in polyacetylene, Phys. Rev. Lett. **42**, 1698 (1979).
[3] B. I. Halperin, Quantized Hall conductance, current-carrying edge states, and the existence of extended states in a two-dimensional disordered potential, Phys. Rev. B **25**, 2185 (1982).
[4] G. E. Volovik, *The Universe in a Helium Droplet* (Oxford University Press, Oxford, 2009).
[5] M. Z. Hasan and C. L. Kane, *Colloquium:* Topological insulators, Rev. Mod. Phys. **82**, 3045 (2010).
[6] A. Dutt, L. Yuan, K. Y. Yang, K. Wang, S. Buddhiraju, J. Vučković, and S. Fan, Creating boundaries along a synthetic frequency dimension, Nat. Commun. **13**, 3377 (2022).
[7] Y. Baum and G. Refael, Setting boundaries with memory: Generation of topological boundary states in Floquet-induced synthetic crystals, Phys. Rev. Lett. **120**, 106402 (2018).
[8] L. Yuan, Y. Shi, and S. Fan, Photonic gauge potential in a system with a synthetic frequency dimension, Opt. Lett. **41**, 741 (2016).
[9] O. Y. Long, K. Wang, A. Dutt, and S. Fan, Time reflection and refraction in synthetic frequency dimension, Phys. Rev. Res. **5**, L012046 (2023).
[10] X.-F. Zhou, X.-W. Luo, S. Wang, G.-C. Guo, X. Zhou, H. Pu, and Z.-W. Zhou, Dynamically manipulating topological physics and edge modes in a single degenerate optical cavity, Phys. Rev. Lett. **118**, 083603 (2017).
[11] T. Ozawa and H. M. Price, Topological quantum matter in synthetic dimensions, Nat. Rev. Phys. **1**, 349 (2019).
[12] L. Yuan, Q. Lin, M. Xiao, and S. Fan, Synthetic dimension in photonics, Optica **5**, 1396 (2018).
[13] E. Lustig and M. Segev, Topological photonics in synthetic dimensions, Adv. Opt. Photon. **13**, 426 (2021).
[14] M. Yang, J.-S. Xu, C.-F. Li, and G.-C. Guo, Simulating topological materials with photonic synthetic dimensions in cavities, Quantum Front. **1**, 10 (2022).
[15] M. Ehrhardt, S. Weidemann, L. J. Maczewsky, M. Heinrich, and A. Szameit, A perspective on synthetic dimensions in photonics, Laser Photonics Rev. **17**, 2200518 (2023).
[16] M. C. Rechtsman, J. M. Zeuner, Y. Plotnik, Y. Lumer, D. Podolsky, F. Dreisow, S. Nolte, M. Segev, and A. Szameit, Photonic Floquet topological insulators, Nature (London) **496**, 196 (2013).
[17] M. S. Rudner, N. H. Lindner, E. Berg, and M. Levin, Anomalous edge states and the bulk-edge correspondence for periodically driven two-dimensional systems, Phys. Rev. X **3**, 031005 (2013).
[18] E. Lustig, S. Weimann, Y. Plotnik, Y. Lumer, M. A. Bandres, A. Szameit, and M. Segev, Photonic topological insulator in synthetic dimensions, Nature (London) **567**, 356 (2019).
[19] G. Pirruccio and G. G. Naumis, Synthetic dimensions in optical cavities and their analogies to two-dimensional materials, Phys. Rev. B **106**, 035155 (2022).
[20] A. Dutt, Q. Lin, L. Yuan, M. Minkov, M. Xiao, and S. Fan, A single photonic cavity with two independent physical synthetic dimensions, Science **367**, 59 (2020).
[21] L. Yuan, A. Dutt, and S. Fan, Synthetic frequency dimensions in dynamically modulated ring resonators, APL Photonics **6**, 071102 (2021).
[22] G. Li, Y. Zheng, A. Dutt, D. Yu, Q. Shan, S. Liu, L. Yuan, S. Fan, and X. Chen, Dynamic band structure measurement in the synthetic space, Sci. Adv. **7**, eabe4335 (2021).

[23] D. Cheng, E. Lustig, K. Wang, and S. Fan, Multi-dimensional band structure spectroscopy in the synthetic frequency dimension, Light Sci. Appl. **12**, 158 (2023).

[24] Z. Liu, L. Zheng, C. Qin, B. Wang, and P. Lu, Multidimensional synthetic frequency lattice in the dynamically modulated waveguides, Opt. Lett. **48**, 3163 (2023).

[25] L. Nemirovsky, M.-I. Cohen, Y. Lumer, E. Lustig, and M. Segev, Synthetic-space photonic topological insulators utilizing dynamically invariant structure, Phys. Rev. Lett. **127**, 093901 (2021).

[26] I. H. Grinberg, M. Lin, C. Harris, W. A. Benalcazar, C. W. Peterson, T. L. Hughes, and G. Bahl, Robust temporal pumping in a magneto-mechanical topological insulator, Nat. Commun. **11**, 974 (2020).

[27] C. Oliver, A. Smith, T. Easton, G. Salerno, V. Guarrera, N. Goldman, G. Barontini, and H. M. Price, Bloch oscillations along a synthetic dimension of atomic trap states, Phys. Rev. Res. **5**, 033001 (2023).

[28] I. Martin, G. Refael, and B. Halperin, Topological frequency conversion in strongly driven quantum systems, Phys. Rev. X **7**, 041008 (2017).

[29] F. Nathan, I. Martin, and G. Refael, Topological frequency conversion in Weyl semimetals, Phys. Rev. Res. **4**, 043060 (2022).

[30] S. K. Sridhar, S. Ghosh, D. Srinivasan, A. R. Miller, and A. Dutt, Quantized topological pumping in Floquet synthetic dimensions with a driven dissipative photonic molecule, Nat. Phys. **20**, 843 (2024).

[31] A. Nagulu, X. Ni, A. Kord, M. Tymchenko, S. Garikapati, A. Alù, and H. Krishnaswamy, Chip-scale Floquet topological insulators for 5G wireless systems, Nat. Electron. **5**, 300 (2022).

[32] A. Stegmaier, H. Brand, S. Imhof, A. Fritzsche, T. Helbig, T. Hofmann, I. Boettcher, M. Greiter, C. H. Lee, G. Bahl, A. Szameit, T. Kießling, R. Thomale, and L. K. Upreti, Realizing efficient topological temporal pumping in electrical circuits, Phys. Rev. Res. **6**, 023010 (2024).

[33] S. Sajad Dabiri and H. Cheraghchi, Electric circuit simulation of Floquet topological insulators in Fourier space, J. Appl. Phys. **134**, 084303 (2023).

[34] W. Zhang, W. Cao, L. Qian, H. Yuan, and X. Zhang, Topolectrical space-time circuits, Nat. Commun. **16**, 198 (2025).

[35] C. H. Lee, S. Imhof, C. Berger, F. Bayer, J. Brehm, L. W. Molenkamp, T. Kiessling, and R. Thomale, Topolectrical circuits, Commun. Phys. **1**, 39 (2018).

[36] T. Helbig, T. Hofmann, C. H. Lee, R. Thomale, S. Imhof, L. W. Molenkamp, and T. Kiessling, Band structure engineering and reconstruction in electric circuit networks, Phys. Rev. B **99**, 161114 (2019).

[37] M. Ezawa, Electric circuits for non-Hermitian Chern insulators, Phys. Rev. B **100**, 081401 (2019).

[38] N. A. Olekhno, E. I. Kretov, A. A. Stepanenko, P. A. Ivanova, V. V. Yaroshenko, E. M. Puhtina, D. S. Filonov, B. Cappello, L. Matekovits, and M. A. Gorlach, Topological edge states of interacting photon pairs emulated in a topolectrical circuit, Nat. Commun. **11**, 1436 (2020).

[39] Y. Wang, H. M. Price, B. Zhang, and Y. D. Chong, Circuit implementation of a four-dimensional topological insulator, Nat. Commun. **11**, 2356 (2020).

[40] T. Helbig, T. Hofmann, S. Imhof, M. Abdelghany, T. Kiessling, L. W. Molenkamp, C. H. Lee, A. Szameit, M. Greiter, and R. Thomale, Generalized bulk–boundary correspondence in non-Hermitian topolectrical circuits, Nat. Phys. **16**, 747 (2020).

[41] T. Hofmann, T. Helbig, F. Schindler, N. Salgo, M. Brzezińska, M. Greiter, T. Kiessling, D. Wolf, A. Vollhardt, A. Kabaši, C. H. Lee, A. Bilušić, R. Thomale, and T. Neupert, Reciprocal skin effect and its realization in a topolectrical circuit, Phys. Rev. Res. **2**, 023265 (2020).

[42] A. Stegmaier, S. Imhof, T. Helbig, T. Hofmann, C. H. Lee, M. Kremer, A. Fritzsche, T. Feichtner, S. Klembt, S. Höfling, I. Boettcher, I. C. Fulga, L. Ma, O. G. Schmidt, M. Greiter, T. Kiessling, A. Szameit, and R. Thomale, Topological defect engineering and $\mathcal{PT}$ symmetry in non-Hermitian electrical circuits, Phys. Rev. Lett. **126**, 215302 (2021).

[43] D. Zou, T. Chen, W. He, J. Bao, C. H. Lee, H. Sun, and X. Zhang, Observation of hybrid higher-order skin-topological effect in non-Hermitian topolectrical circuits, Nat. Commun. **12**, 7201 (2021).

[44] K. Yatsugi, T. Yoshida, T. Mizoguchi, Y. Kuno, H. Iizuka, Y. Tadokoro, and Y. Hatsugai, Observation of bulk-edge correspondence in topological pumping based on a tunable electric circuit, Commun. Phys. **5**, 180 (2022).

[45] T. Kotwal, F. Moseley, A. Stegmaier, S. Imhof, H. Brand, T. Kießling, R. Thomale, H. Ronellenfitsch, and J. Dunkel, Active topolectrical circuits, Proc. Natl. Acad. Sci. USA **118**, e2106411118 (2021).

[46] See Supplemental Material at http://link.aps.org/supplemental/10.1103/6n5m-wvs7 for Appendix containing a detailed derivation of all circuit dynamics and a complete listing of the explicit components used to build the Floquet SSH circuit.

[47] T. Oka and S. Kitamura, Floquet engineering of quantum materials, Annu. Rev. Condens. Matter Phys. **10**, 387 (2019).

[48] X. Qiao, L. Wang, G. Li, X. Chen, and L. Yuan, Topological degeneracy breaking in synthetic frequency lattice by Floquet engineering, Nanophotonics **12**, 3807 (2023).

[49] G. Li, L. Wang, R. Ye, Y. Zheng, D.-W. Wang, X.-J. Liu, A. Dutt, L. Yuan, and X. Chen, Direct extraction of topological Zak phase with the synthetic dimension, Light Sci. Appl. **12**, 81 (2023).

[50] Y. Song, S. Ke, Y. Chen, and M. Wang, Mode-locking in anti-PT symmetric frequency lattices, Appl. Phys. Lett. **122**, 151106 (2023).